J. Fluid Mech. (1979), *vol.* 94, *part* 2, *pp.* 243–268
Printed in Great Britain

The response of a turbulent boundary layer to lateral divergence

By A. J. SMITS†, J. A. EATON‡ AND P. BRADSHAW

Department of Aeronautics, Imperial College, London

(Received 21 August 1978)

Measurements have been made in the flow over an axisymmetric cylinder–flare body, in which the boundary layer developed in axial flow over a circular cylinder before diverging over a conical flare. The lateral divergence, and the concave curvature in the transition section between the cylinder and the flare, both tend to destabilize the turbulence. Well downstream of the transition section, the changes in turbulence structure are still significant and can be attributed to lateral divergence alone. The results confirm that lateral divergence alters the structural parameters in much the same way as longitudinal curvature, and can be allowed for by similar empirical formulae. The interaction between curvature and divergence effects in the transition section leads to qualitative differences between the behaviour of the present flow, in which the turbulence intensity is increased everywhere, and the results of Smits, Young & Bradshaw (1979) for a two-dimensional flow with the same curvature but no divergence, in which an unexpected collapse of the turbulence occurred downstream of the curved region.

1. Introduction

This paper is one of a series on 'complex' turbulent flows (defined as shear layers with complicating influences like distortion by extra rates of strain or interaction with another turbulence field). For an introduction to the subject see the companion paper by Smits *et al.* (1979), hereafter referred to as I. The present experiment was intended to investigate the effect of lateral divergence, leading to an extra component of mean strain rate equal to $\partial W/\partial z$ in x, y, z axes on a boundary layer whose basic strain rate is the simple shear $\partial U/\partial y$. As pointed out in I, the main question to be answered is how the extra rate of strain affects the dimensionless parameters of the turbulence structure, and also their computational counterparts, the empirical constants or functions appearing in calculation methods. The effects on the turbulence structure parameters are likely to be more important than the explicit extra terms in the exact Reynolds-stress transport equations (for example the extra production term $-\overline{w^2}\partial W/\partial z$ in the turbulent energy equation for a diverging flow). Furthermore, the structural effects may oppose the effects of the explicit extra terms: lateral divergence ($\partial W/\partial z > 0$) is known to increase turbulent energy but makes the above-mentioned production term negative. In what follows we will refer to divergence or convergence effects as 'divergence effects' for brevity, making the sign clear when necessary.

† Present address; Mechanical Engineering Department, University of Melbourne.
‡ Present address; Engineering Department, University of Leicester.

0022–1120/79/4260–7240 $02.00

A positive value of $\partial W/\partial z$ must be balanced, in incompressible flow, by negative values of $\partial U/\partial x$ or $\partial V/\partial y$ or both, and without a long series of experiments it is not logically possible to attribute any observed effects of the extra strain rate to $\partial W/\partial z$ rather than $\partial U/\partial x$ or $\partial V/\partial y$. In most of the previous work on lateral divergence, and in the experiment described below, streamwise accelerations have been fairly small and $\partial W/\partial z$ has been balanced mainly by $\partial V/\partial y$.† Now Townsend (1956, p. 188) attributed the reduction of large-eddy strength in a two-dimensional jet, compared to that in a wake, to the effect of negative $\partial V/\partial y$ in the jet (where it is balanced by $\partial U/\partial x$): if this attribution is correct and generally valid, it implies that in a typical diverging flow the effects of positive $\partial W/\partial z$ in augmenting turbulent activity outweigh the contrary effects of the negative $\partial V/\partial y$. As suggested by J. E. Green (private communication) there is probably a close analogy between the effect of positive $\partial W/\partial z$ in decreasing the cross-sectional area of a fluid element in the x, y plane and thus increasing its z-component vorticity, and the effect of bulk compression, extra strain rate $-(\partial U/\partial x+\partial V/\partial y)$, in two-dimensional compressible flow. Intensification of turbulent activity by bulk compression explains some curious features of supersonic turbulent boundary layers, including the *increase* of skin-friction coefficient that results from application of a moderate adverse pressure gradient (Bradshaw 1974; but see also Rubesin *et al.* 1977). Here, $\partial U/\partial x$ is much smaller than $\partial V/\partial y$ at high Mach number so that again the vorticity-intensification effect outweighs any effect of $\partial V/\partial y$ as such.

Nearly all three-dimensional or axisymmetric shear layers are affected by lateral divergence of the mean streamlines, and several experiments (Reynolds 1963; Keffer 1965, 1967; Winter, Rotta & Smith 1968; Crabbe 1971; Patel, Nakayama & Damian 1974; Agrell & White 1974; Brederode & Bradshaw 1978) have shown explicitly or implicitly that the turbulence structure is affected. (There are many other experiments on converging or diverging flows in the literature, which for one reason or another do not yield currently useful information on structural effects.) Calculations by Green, Weeks & Brooman (1972) and others suggest that the effect of a given strain rate $\partial W/\partial z$ on the turbulence structure is of the same order as that of an equal value of $\partial V/\partial x$, the extra strain rate imposed by streamline curvature. However, there seems to be no experiment designed to investigate a laterally diverging boundary layer in the absence of other special effects like three-dimensionality or transverse curvature: Reynolds and Keffer studied wakes with nominally collinear divergence (or convergence); Winter *et al.* (1968) studied the boundary layer on a waisted body of revolution in the presence of significant transverse curvature and also – as shown by Green *et al.* (1972) – with significant effects of streamwise curvature, lateral divergence, convergence *and* bulk compression; Johnston (1960) and Crabbe (1971) studied three-dimensional diverging boundary layers similar to that at the attachment line of a swept wing; Patel *et al.* (1974) and Agrell & White (1974) studied the flow over a streamline body of revolution, necessarily in the presence of strong transverse curvature and significant streamline curvature near the tail; Bansod & Bradshaw (1972) studied the generation of extremely strong streamwise vorticity in a laterally converging flow in an S-shaped duct; and Brederode & Bradshaw (1978) investigated the centre-plane boundary layer in a square duct, subject to lateral convergence due to growth of side-wall boundary layers. The only configuration that gives pure

† So that the net production term (still negative) is $(\overline{v^2}-\overline{w^2})\,\partial W/\partial z$.

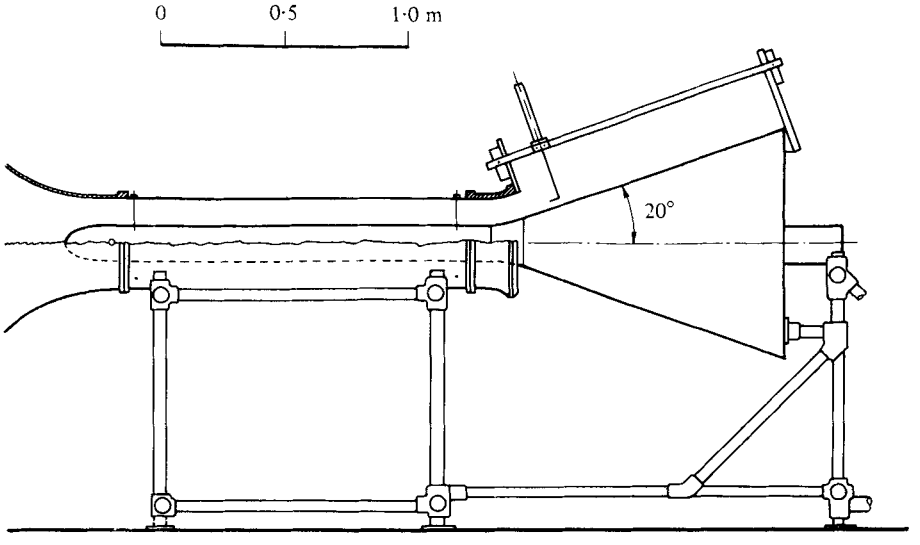

FIGURE 1. Side view of cylinder-flare model in blower rig.
Measurements all made on top centre-line.

divergence and zero longitudinal vorticity is a circular cone, but if the origin of the boundary layer is at the apex of the cone the rate-of-strain parameter $(\partial W/\partial z)/(\partial U/\partial y)$ does not exceed about 0·03 in mid-layer whatever the cone angle.

In order to achieve a larger rate-of-strain ratio than is attainable on a cone, we have studied the boundary layer on an axisymmetric 'cylinder-flare' body (figure 1) in which the boundary layer initially grows on a cylinder in axial flow and then passes to a conically diverging flare with an included angle of 40°. Necessarily, streamline curvature occurs in the transition section between cylinder and flare, but our hope was that the effects of streamline curvature would die out soon enough for divergence effects to be studied in near-isolation on the downstream part of the flare. In order to assess, and if possible subtract, the effects of streamline curvature alone, a comparison experiment (case CC20C of I) was performed on the boundary layer in a two-dimensional 20 degree concave bend with the same side view, and roughly the same initial boundary-layer thickness, as the cylinder-flare body. Quantitative subtraction of streamline curvature effects proved not to be possible, because of an apparent nonlinear interaction between curvature and divergence, but the qualitative picture is clear.

In startling contrast to I, where concave streamline curvature in nominally two-dimensional flow led to development of strong spanwise variations, plausibly ascribable to longitudinal vortices, streamline curvature accompanied by lateral divergence seems if anything to reduce pre-existing circumferential variations. Explanations can be offered but not as yet proved; more information about vortex formation in nominally two-dimensional flow is needed, and further work is in progress. However the absence of longitudinal vortices on the cylinder-flare body simplifies the interpretation of results. The continuing divergence prevents the collapse of turbulent

activity found downstream of the concave bends in I, and it can be claimed with reasonable confidence that the differences between the boundary layer on the downstream part of the flare and a self-preserving constant-pressure boundary layer are due to divergence effects, rather than to memories of the curvature further upstream. This claim applies also to the effects of transverse curvature; δ/r at the start of the transition section was 0·25, which itself appeared to be too small to affect the boundary layer significantly, while at the last measurement station δ/r was barely 0·1. The rate-of-strain ratio $(\partial W/\partial z)/(\partial U/\partial y)$ is equal to $(U/r)\,dr/dx/(\partial U/\partial y)$ and since dr/dx is constant the ratio varies roughly as $1/r$. At the last measurement station the ratio is about 0·1 in mid-layer while, as a simple example of the strength of divergence effects, the apparent mixing length in the outer layer at this station is about twice as large as in a two-dimensional boundary layer of the same thickness.

Section 2 describes the apparatus and techniques, and § 3 presents the results, which include sufficiently detailed turbulence measurements to permit the evaluation of turbulent energy and shear-stress balances. Section 4 is a discussion of the results, concentrating mainly on the dimensionless structure parameters and the transport-equation balances. The implications of the results for turbulence modelling are not discussed in detail; this will be done in a later paper.

2. Apparatus and techniques

The cylinder-flare body (figure 1) has a cylindrical section 152·4 mm in diameter and 1460 mm long, preceded by a streamlined nose 160 mm long and followed by a flare of 20° half-angle. The radius of curvature of the transition section between the cylinder and the flare is 254 mm and it follows that the imaginary apex of the flare lies on the axis 164 mm upstream of the start of the transition section. Measurement stations (figure 2*a*) are defined at intervals of 25·4 mm measured along the surface, the first being 146 mm upstream of the start of the transition section, which has an arc length of 89 mm. For ease of comparison with I, the origin of the distance s, measured along the surface, is taken at the end of the transition section, 267 mm from the imaginary apex of the conical flare. Thus $(1/r)\,dr/ds = 1/(s+267)$ for $s > 0$.

The body is mounted in the 355·6 mm diameter working section of a blower wind tunnel, identical with that used in I except for the contraction and working section: the body is supported by sets of four 1·4 mm wires, one set at each end (figure 1). The working section terminates in a short bell surrounding the transition section of the centre-body, designed by eye to minimize the pressure peak on the transition section of the centre-body. The annular mixing layer that forms downstream of the exit bell (figure 2*a*) intersects the boundary layer on the centre-body flare at about $s = 450$ mm; no serious measurements were made downstream of $s = 375$ mm but the skin friction coefficient is little affected up to $s = 600$ mm at least.

The tunnel reference velocity U_{ref} was taken as the free-stream speed a short distance downstream of the nose, at $s = -1650$ mm, and was set at 38 m s^{-1} ($U_{\mathrm{ref}}/\nu \simeq 2{\cdot}57 \times 10^6$ m^{-1}). The free-stream speed increased down the working section to about $1{\cdot}07U_{\mathrm{ref}}$ near the start of the transition section, because of boundary-layer growth; the pressure-gradient parameter $(\delta^*/\tau_w)\,dp/dx$ is only about $-0{\cdot}02$ at this point, and the skin-friction coefficient is negligibly different from the value in a constant-pressure boundary layer at the same Reynolds number, while the Coles wake parameter Π is

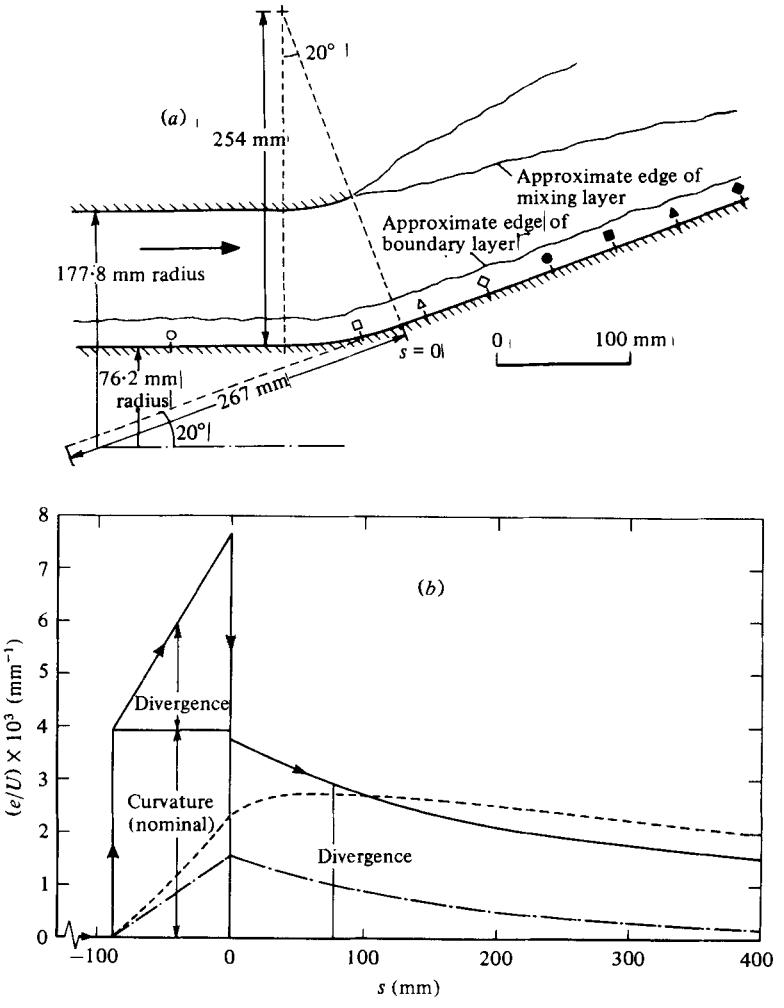

FIGURE 2(*a*, *b*). For legend see next page.

also very close to the constant-pressure value of 0·58. The boundary-layer thickness is *not* exactly the same as at the entry to the 20° bend in I; but recall from I that the state of the turbulence at exit from a sharp bend depends mainly on the turning angle and less on the ratio of the boundary-layer thickness to the radius of longitudinal curvature R.

Measurement techniques and procedures were generally as in I; the only major difference is that all three fluctuating velocity components were measured, in the upper half of a diametral vertical plane, in the present work.

Figure 2(*b*) shows the extra strain rates, calculated from the body geometry. The values for curvature are based on the surface curvature rather than that of the streamlines, and except very close to the surface the plot of the true curvature contribution to e/U will be a bell-shaped curve of area equal to the rectangle marked 'curvature' in figure 2(*b*) but extending over a somewhat larger range of s. Except in the immediate neighbourhood of the curved transition region the response of the flow

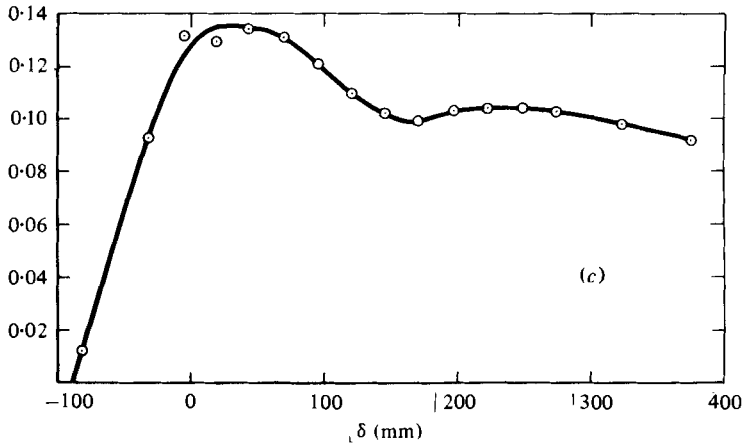

FIGURE 2. Geometry and extra strain rates. (*a*) Details of measurement region; see table 1 for symbol key. (*b*) Extra strain rate e: for curvature, $e = U/R = \partial V/\partial x$; for divergence, $e = (U/r)\, dr/ds = \partial W/\partial z$. The superposition of the two is for illustration only. ——, actual strain rates; · · · · ·, effective (total) strain rate (10δ lag); —·—·—, curvature contribution to effective strain rate. (*c*) $(\partial W/\partial z)/\partial U/\partial y$ at $y = 0{\cdot}5\delta$.

depends mainly on the total turning angle rather than the distribution of curvature, so that the discrepancy is not important for present purposes. The curvature and divergence contributions have been superimposed for illustration; this would be exactly valid only if the response of the flow was linearly proportional to the extra strain rate with the same constant of proportionality for curvature and for divergence, but this is a good first approximation. To demonstrate that the memory of curvature effects is small at large s, we have plotted in figure 2(*b*) the 'effective' strain rate e_{eff}, defined by the lag equation

$$\frac{de_{\text{eff}}}{dx} = \frac{e - e_{\text{eff}}}{10\delta}, \tag{1}$$

which is a simplified version of equation (2) of I. Use of (1) in calculation methods produces a significant improvement in prediction of effects of short regions of extra strain rate so that it is at least qualitatively useful. The curvature contribution to the effective strain rate, the chain-dotted line in figure 2(*b*), is a fairly small fraction of the total effective strain rate (dotted line) for $s > 200$ mm say, so that (accepting the above-mentioned conclusion that a given $\partial W/\partial z$ produces the same order of effect as the same value of $\partial V/\partial x$) the structural changes observed in this region are attributable primarily to divergence, with comparatively small effects of curvature.

Figure 2(*c*) shows the (unlagged) extra-strain-rate parameter $(\partial W/\partial z)/(\partial U/\partial y)$ evaluated at $y/\delta = 0{\cdot}5$ using the profile data presented below.

3. Results

The pressure distribution is shown in figure 3. The alternating pressure gradients in the region of the bend result from the failure of the bell (figure 1) to cancel the curvature-induced pressure entirely. The maximum value of the pressure-gradient parameter $(\delta^*/\tau_w)\, dp/dx$, just downstream of the curved region, is about 2·4; although the pressure gradients cause quite large excursions in skin-friction coefficient (figure 4)

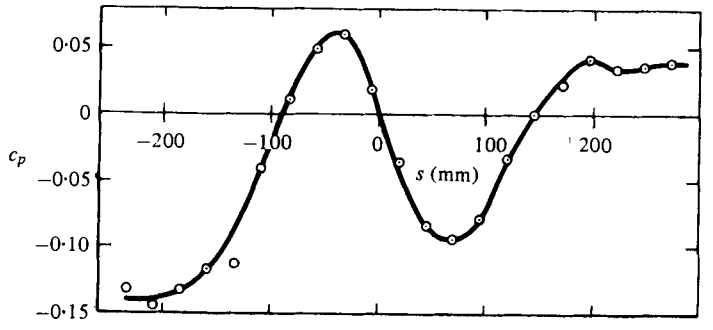

FIGURE 3. Surface pressure distribution: $c_p = (p - p_{ref})/\frac{1}{2}\rho U_{ref}^2$.

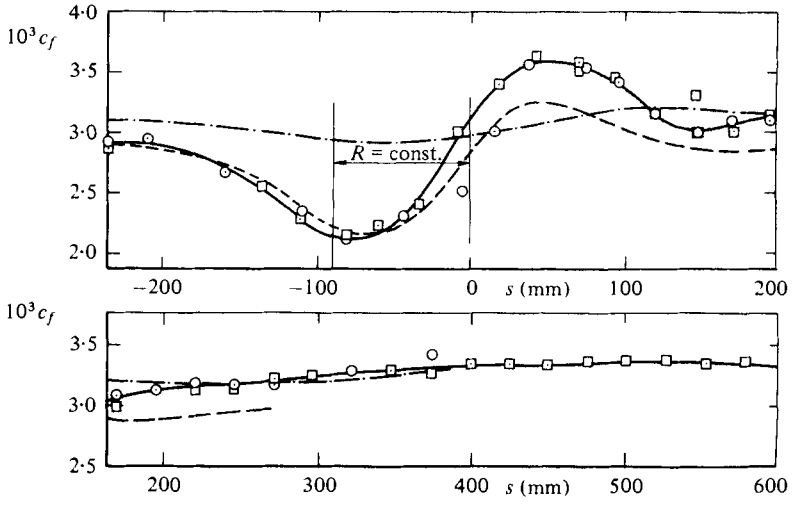

FIGURE 4. Skin-friction coefficient, $c_f \equiv \tau_w/(0{\cdot}5\rho U_e^2)$. ⊙, logarithmic law; ⊡, Preston-tube measurement; – – –, calculation without allowance for extra strain rates in turbulence model; –·–·–, constant-pressure c_f for same R_θ.

their effects on the turbulence will be confined to the inner layer while the net decrease in free stream velocity through the bend is only about 10 per cent. As in I, we take the position that the effect of moderate pressure gradients on the dimensionless structural parameters of the turbulence is small, in the sense that boundary layers in moderate, arbitrary pressure gradients can be predicted satisfactorily by calculation methods assuming constant values for structural parameters. Passing support for this statement is provided by the calculation for the present flow shown in figure 4: the calculation was made by the method of Bradshaw and co-workers (Bradshaw & Unsworth 1974) without allowance for effects of curvature or divergence on the turbulence structure, and it can be seen that the discrepancy between calculation and experiment increases smoothly through the bend, as expected if the discrepancy is due mainly to cumulative extra-strain effects rather than the alternating effects of pressure gradient. The skin-friction coefficient starts to increase at $s \simeq 150$ mm, somewhat before the end of the region of adverse pressure gradient. It rises slightly but significantly above the constant-pressure value for the local value of $U_e\theta/\nu$, also plotted in figure 4, but a more useful comparison for the assessment of extra-strain effects is with the *calculation*.

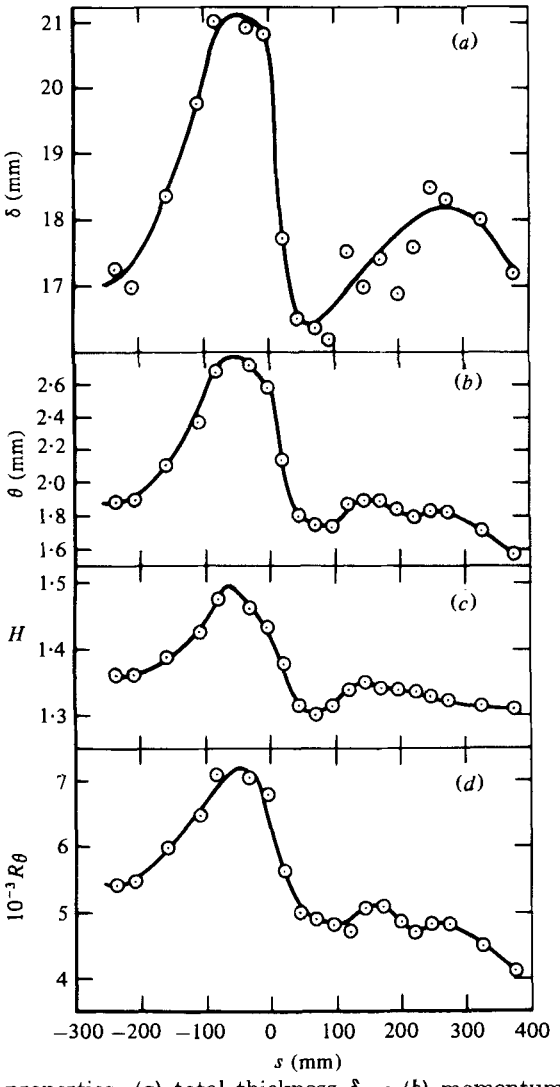

FIGURE 5. Integral properties: (*a*) total thickness δ_{995}; (*b*) momentum thickness θ; (*c*) shape parameter H, δ^*/θ; (*d*) momentum-thickness Reynolds number $U_e\theta/\nu$.

The accuracy of the skin-friction measurements is indicated by general agreement to within about 2 per cent between values obtained from Preston tube readings and those deduced from logarithmic velocity profiles, except for the profiles at $s = 4{\cdot}6$ and $s = 19$ where the logarithmic region is not well enough defined for the curve-fitting procedure used in the data analysis.

Integral parameters obtained from the mean velocity profiles are shown in figure 5. The main effect of lateral divergence on the flow is a tendency for the boundary-layer thickness to decrease: in fact the momentum thickness happens to remain nearly constant for some distance downstream of the bend. The momentum-thickness Reynolds number at the last measurement station is still slightly over 4000 and low-Reynolds-number effects are therefore ignored in the data analysis. Values of the shape parameter are much lower, and the skin friction coefficient is somewhat higher,

Station	Symbol	s (mm)	δ_{995} (mm)	U_e/U_{ref}
6	○	−159	18·53	1·094
11	□	−32	21·20	1·003
14	△	19	17·58	1·024
16	◇	70	16·35	1·077
18	●	121	16·57	1·039
20	■	171	17·33	1·010
22	▲	222	17·57	1·011
24	◆	273	18·25	1·011

TABLE 1. Free stream velocity, boundary-layer thickness δ_{995}, and symbol key for turbulence measurements. δ_{995} values were measured during same series of runs as turbulence quantities. Figure 5 shows an earlier, more complete set.

than in constant-pressure two-dimensional flow at the same Reynolds number. The boundary-layer thickness $\delta \equiv \delta_{995}$, defined as the distance from the surface at which $U/U_e = 0{\cdot}995$, is given in table 1; it is used to scale most of the profiles presented below.

Figure 6(*a*) shows the circumferential variation of Preston tube readings, which can be taken as roughly proportional to skin-friction coefficient. Large excursions occur in the wakes of the four wires which hold the centre-body in place, as might be expected. The regions of high skin friction either side of the wire wake result from the horseshoe vortex wrapped round each support wire; although the increase in height of these peaks as the flow passes through the curved transition section is probably attributable to the effects of streamline curvature on longitudinal vortices, the peaks would appear even on a flat surface. The excursions elsewhere on the circumference do not seem to be significantly increased by the bend (compare $s = -108$ mm and $s = 44$ mm) and nowhere exceed about ± 4 per cent whereas in I the excursions downstream of two-dimensional bends exceeded ± 10 per cent. Some separate and more detailed measurements, including local static pressure so that accurate values of c_f could be deduced, were made over a circumferential distance of about 25° near the top generator. The results are shown in figure 6(*b*); circumferential variations *decrease* significantly with increasing distance downstream (results at the last station may have been affected by the merging mixing layer). The bars on the figure show the boundary-layer thickness at each station, on the angle scale; if longitudinal vortices occurred the period of the resulting circumferential variation would be about 2δ. It appears from this that steady longitudinal vortices are not formed in the present case†: it is possible that *unsteady* vortices form, and this question will be discussed below. In view of the absence of any tendency for c_f to amplify, no further circumferential traverses have been made: indeed, the results presented in figure 6 were taken only as a preliminary check on circumferential variations and may be somewhat scattered, thus exaggerating the excursions of c_f. The present results do not include any two-point correlations and it has therefore not been possible to see whether the large eddies have an unusually high level of (fluctuating) *circumferential* vorticity, the likely effect of divergence.

† Most observations of curvature-induced vortices have been made on tunnel walls, but the pioneering measurements of Tani (1962) were made on a body mounted in mid-tunnel. Hypothetical peculiarities in tunnel screens, confined to the region near the tunnel walls, are therefore not a sufficient cause of vortices.

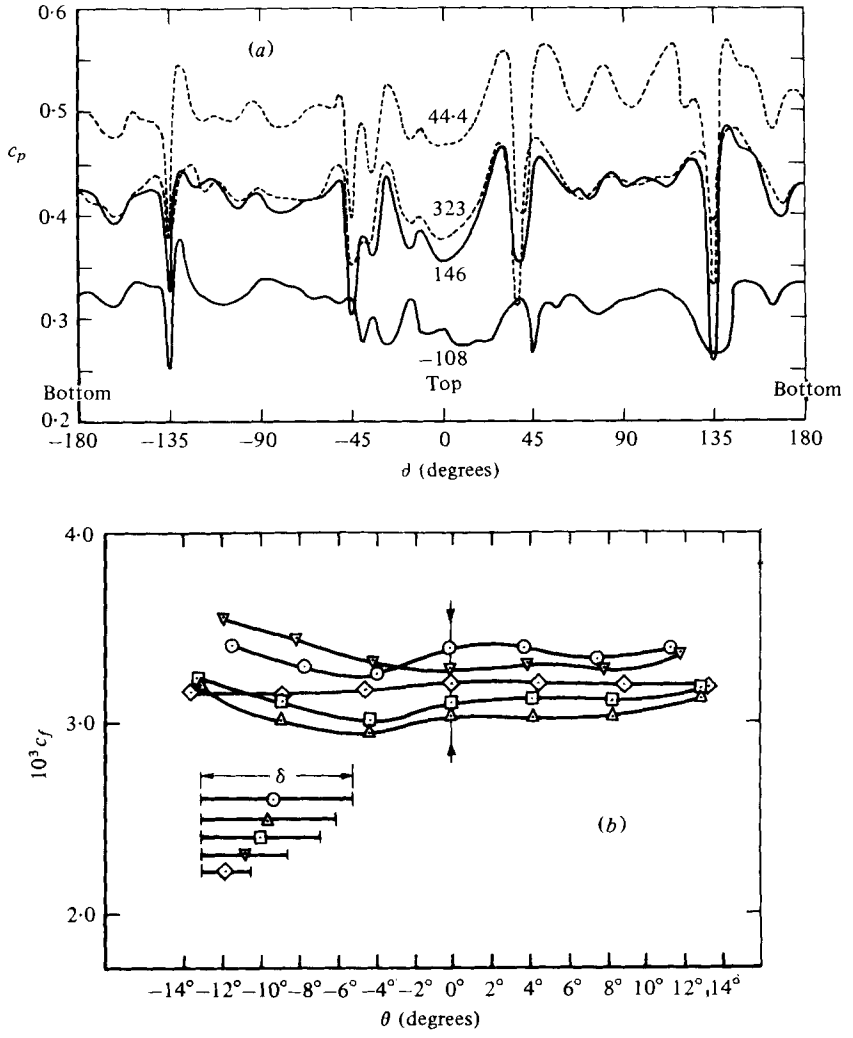

FIGURE 6. Circumferential variations of c_f; large excursions near $\pm 45°$ and $\pm 135°$ are wakes of support wires. (*a*) Preston-tube pressure coefficients around full circumference. (*b*) Skin-friction coefficients near top generator, ⊙, $s = 95$ mm; △, 146; □, 222; ▽, 375; ◇, 679.

Mean 'velocity' profiles are shown in figure 7. The quantity labelled U is actually $\{2(P-p_w)/\rho\}^{\frac{1}{2}}$; that is, U is deduced from the local total pressure and the *wall* static pressure. Static-pressure measurements were not made within the stream. Differences between U and the true velocity are negligible except for the profiles in the curved transition section ($s = -82{\cdot}6$, $-32{\cdot}0$ and $-4{\cdot}6$ mm) where the static-pressure difference across the boundary layer will be somewhat less than the value $\rho U_e^2 \delta/R$ deduced from the assumption that the velocity is U_e and the streamline curvature $1/R$ everywhere. The largest value of $\delta \equiv \delta_{995}$ is 21·4 mm at $s = -32$ mm: $\rho U_e^2 \delta/R$ is then $0{\cdot}17 \times \frac{1}{2}\rho U_e^2$ and the actual value of $p_w - p_\delta$ is likely to be about half this, judging by the calculations of Mahgoub & Bradshaw (1977) for the two-dimensional bends of I. Thus the difference between U and the actual velocity at $y = \delta$ is likely to be no more than 4 per cent at the most critical station while the difference in the inner layer,

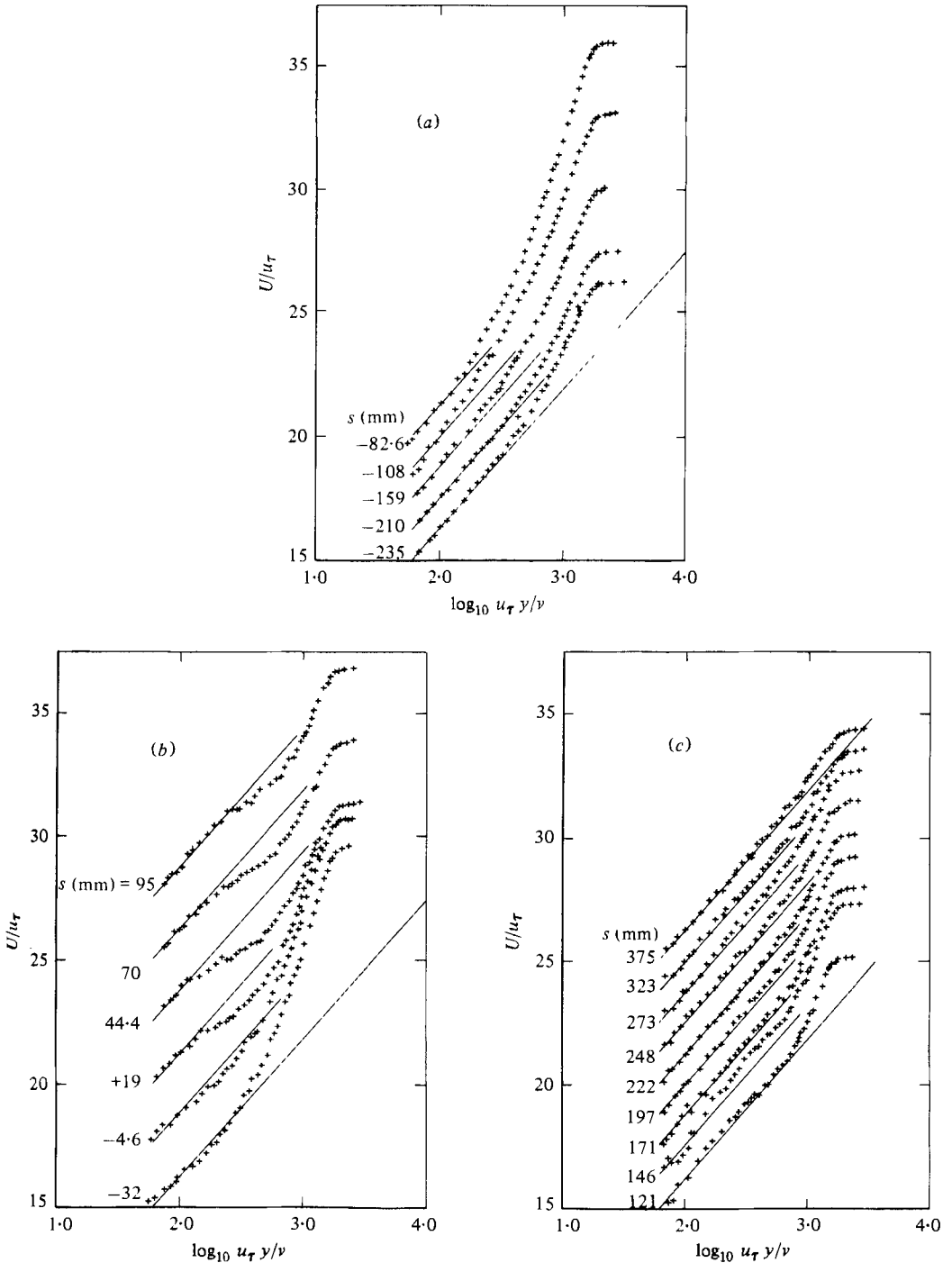

FIGURE 7. U-component mean velocity profiles (logarithmic plot). (*a*) $s = -235$ to $-82{\cdot}6$ mm (curved transition section starts at $s = -88{\cdot}6$): scale of U/u_τ is for $s = -235$; other profiles shifted upwards successively by 1·25 units. (*b*) $s = -32$ to 95 mm, showing appearance of dip in logarithmic law: scale of U/u_τ is for $s = -32$; other profiles shifted upwards successively by 2·5 units. (*c*) $s = 121$ to 375 mm, showing persistence of small 'wake' component: scale of U/u_τ is for $s = 121$; other profiles shifted upwards successively by 1·25 units.

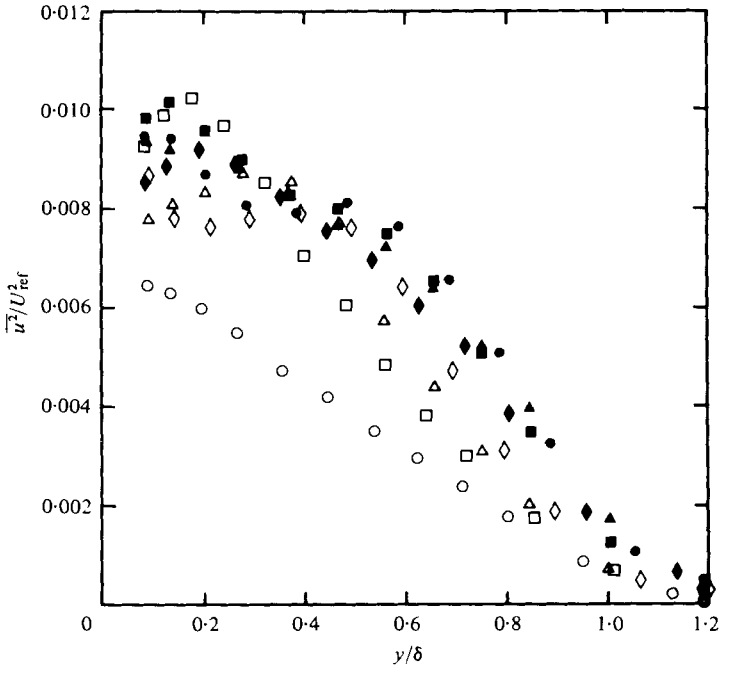

FIGURE 8. Mean-square u-component intensity profiles. For key to symbols see table 1.

$y/\delta < 0{\cdot}2$ say, is negligible. The length of the bend is 89 mm or about 5δ; over this short region the total pressure on a given streamline is almost conserved (whatever the pressure gradient) and therefore $U(y)$ as defined above, or strictly $U(\psi)$, where ψ is the stream function, is a more relevant quantity than the true velocity, which just reflects quasi-inviscid distortion by the pressure gradients. This view is supported by the U profiles, which show a steady trend in and downstream of the bend. The Coles wake parameter Π, proportional to the maximum deviation of the velocity profile above the logarithmic law, increases to a maximum at $z = -82{\cdot}6$, where the adverse pressure gradient is a maximum, and then decreases smoothly. The wake parameter is so strongly dependent on u_τ that it is not an unambiguous indicator of the state of the outer layer, but for present purposes it is an adequate global parameter to demonstrate the smooth variation of the pseudo-velocity U.

The dip below the logarithmic law, shown in I to be the result of an increase in eddy length scale due to the destabilizing effects of concave curvature (presumably assisted in the present case by the destabilizing effects of lateral divergence) persists until after station 17, some $6\delta_0$ downstream of the end of the bend, but thereafter the profile shape is near-normal, with a rather small wake component. In all profiles the logarithmic region near the wall is extensive enough for adequately reliable values of c_f to be deduced.

Figures 8–11 show the Reynolds normal and shear stresses, normalized by $U_{\rm ref}^2$ and plotted against y/δ for easy identification of trends. The sudden collapse found downstream of the two-dimensional concave bends in I is absent: turbulence levels decay very slowly downstream of the bend and are still well above the initial values even at the last station; far enough downstream, the profiles will return to approximately

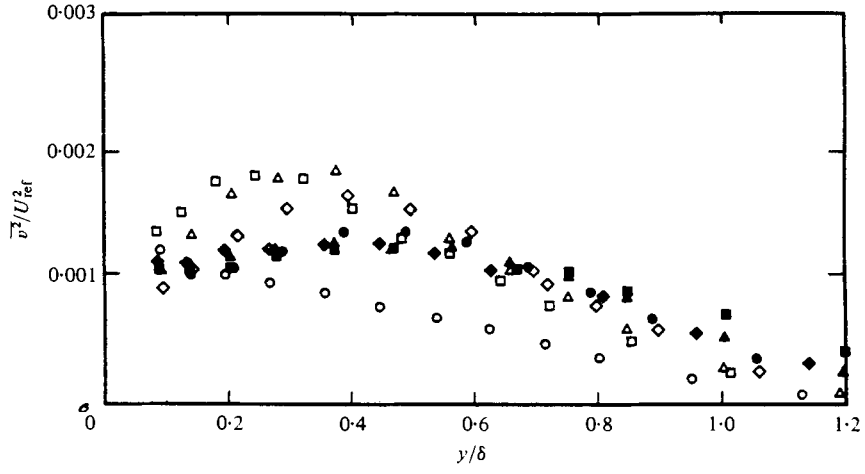

FIGURE 9. Mean-square v-component intensity profiles.
For key to symbols see table 1.

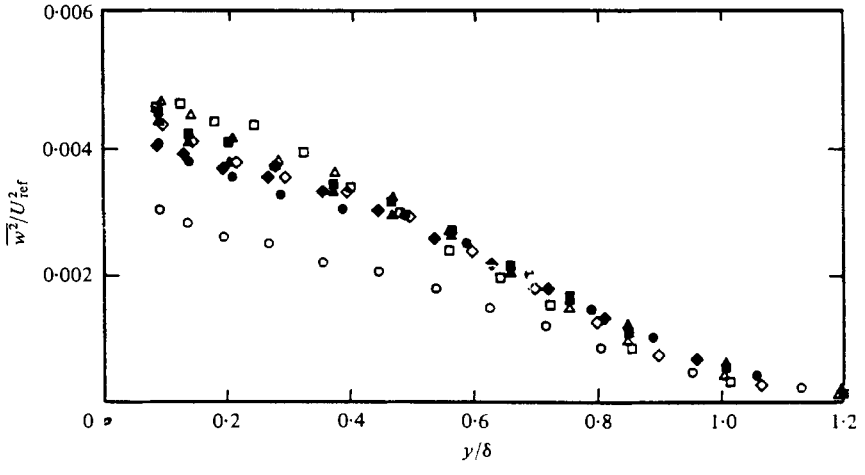

FIGURE 10. Mean square w-component intensity profiles.
For key to symbols see table 1.

their initial shapes, albeit scaling on u_τ^2 rather than U_{ref}^2. The most notable feature of the profiles is the outward progression of the decaying peak. Values of $\overline{uv}$ and $\overline{v^2}$ at $s = 171$ mm (filled squares) are obviously too low but the general trend is clear.

The same feature of an outward-progressing peak is found in the triple products, figures 12–14: qualitatively it results from the development of large-eddy eruptions.

Further derived results and calculations are presented below.

4. Discussion

As mentioned above, the effects of longitudinal curvature and lateral divergence (hereafter referred to simply as 'curvature' and 'divergence') proved to be too large for the effect of divergence to be taken simply as the difference between the present results and the results for the 20° two-dimensional concave bend in I. However a

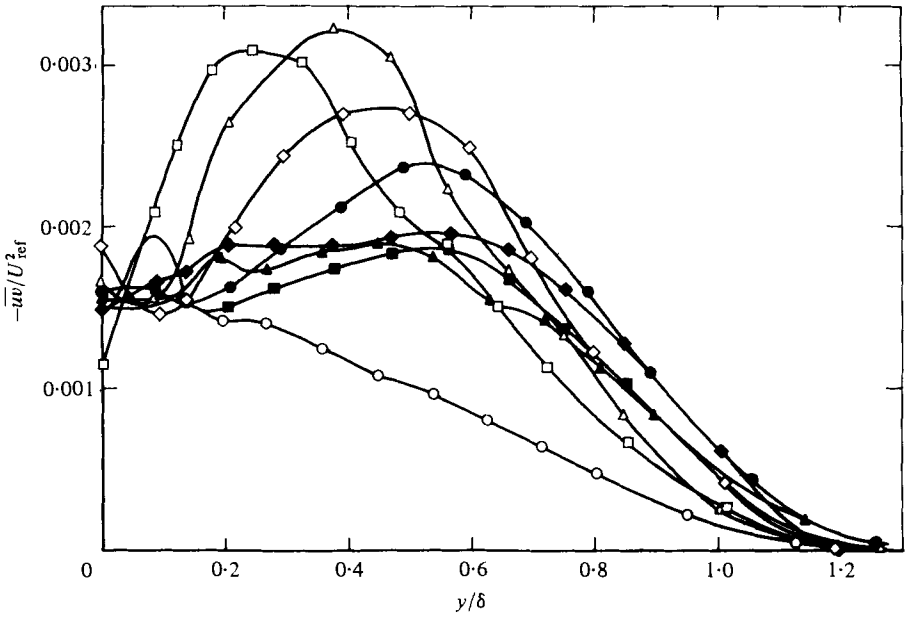

FIGURE 11. Shear-stress profiles. For key to symbols see table 1.

qualitative comparison between the two experiments is the best way of introducing the present results.

The most obvious difference between the present results and the two-dimensional bend results is that the strong spanwise variations due to quasi-steady longitudinal vortices are absent here. Indeed the pre-existing spanwise variations, resulting from non-uniformity in the tunnel stream, actually seem to decrease in the region of divergence. It cannot be proved that this difference between the two-dimensional and axisymmetric results is real, rather than a consequence of the difference in the initial spanwise variations, but all the evidence suggests that quasi-steady longitudinal vortices are absent from the cylinder-flare diverging flow. If this is so the remaining possibilities are that longitudinal vortices, presumably formed in the curved region, are still present in the conically diverging region but have no preferred circumferential position† and therefore produce no circumferential variation of mean values; or that no longitudinal vortices worthy of the name are present. Of course the ensemble-average large eddy in a plane boundary layer still contains longitudinal vorticity but the streamwise coherence length of the latter is of the order of the boundary-layer thickness instead of many times this as in the case of a longitudinal vortex proper.

The second main difference between the diverging flow and the flow in the two-dimensional concave bend is that the high turbulence levels generated in the curved region persist in the conically diverging region, decaying only slowly as the divergence parameter $(\partial W/\partial z)/(\partial U/\partial y)$ decreases. This behaviour was expected; the unexpected behaviour was the rapid decrease of turbulent activity below the initial level in the case of the two-dimensional bend, rather than a monotonic return to the constant-pressure self-preserving state. If one ignored the strong hints of interaction between

† The narrowness of the support-wire wakes implies that circumferential wandering is small, but successive vortices might *originate* at different circumferential positions.

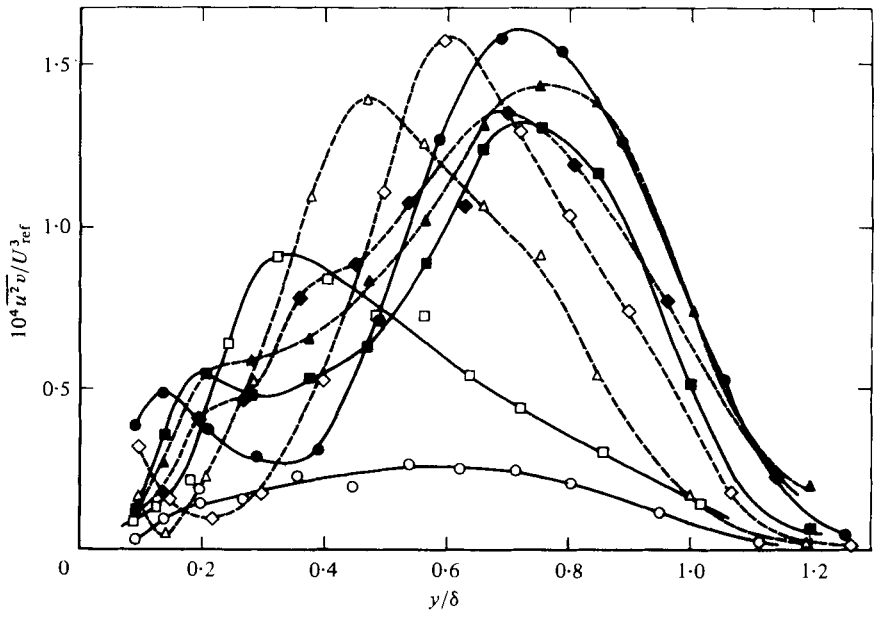

FIGURE 12. Profiles of triple product $\overline{u^2v}$. For key to symbols see table 1.

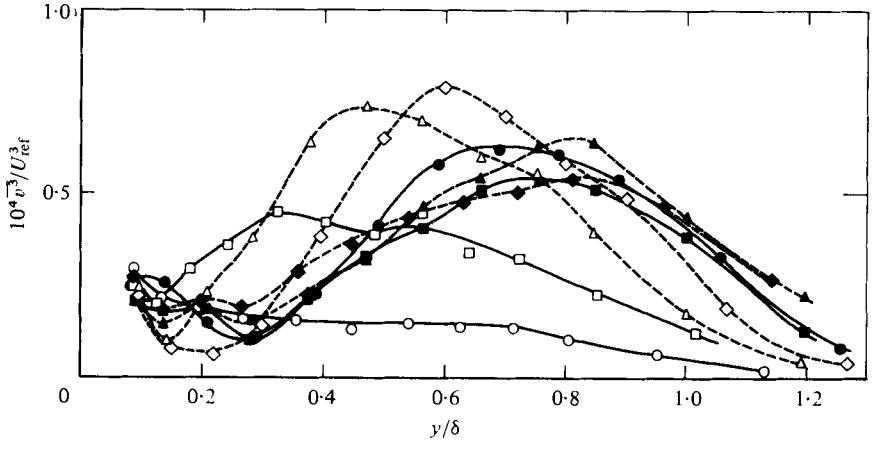

FIGURE 13. Profiles of triple product $\overline{v^3}$. For key to symbols see table 1.

the effects of curvature and the effects of divergence given by the above-mentioned absence of longitudinal vortices, one would attribute the whole differences between the two flows to the effects of divergence acting alone, and deduce that those effects are very large. Even a more reasonable estimate making a generous allowance for the interaction – say, an assumption that, far downstream of the curved region, the effect of divergence alone is equal to the difference between the observed flow and the constant-pressure self-preserving state – leads to the conclusion that divergence effects are highly significant.

One must distinguish between changes in dimensional properties, such as intensity and shear stress, and changes in dimensionless properties such as the ratio of shear

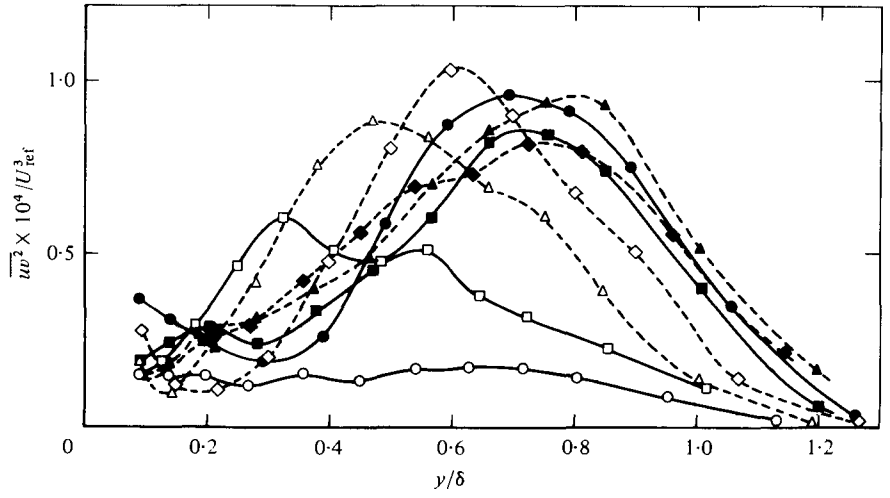

FIGURE 14. Profiles of triple product $\overline{uv^2}$. For key to symbols see table 1.

stress to turbulent kinetic energy. Changes of the latter sort imply changes in the empirical input to calculation methods, and obviously some structural changes must occur if the effect of an extra strain rate is larger than the effect of the explicit extra terms it introduces into the Reynolds-stress transport equations. The main part of the discussion is concerned with structural parameters, but is preceded by comments on dimensional quantities such as the mean velocity and Reynolds stresses.

The mean velocity profiles (figures 7*a–c*) show the same dip below the logarithmic law as the two-dimensional bend results, but it vanishes much more quickly, about six initial boundary-layer thicknesses downstream of the end of the curved region, i.e. at $s \simeq 6\delta$. The wake component of the velocity profile increases to a maximum at $s \simeq 7$–8δ, and thereafter decreases. The momentum-thickness Reynolds number decreases slowly over most of the conically diverging region but is still slightly over 4000 at the last measurement station ($s \sim 15\delta$) so that the decrease in wake component cannot be attributed to the low-Reynolds-number effects documented by Coles (1962), which would predict a decrease in $\Delta u/u_\tau$ of only about 0·14 at $U_e\,\theta/\nu = 4000$. Crudely, we expect small values of wake component (low H) to result from larger-than-usual negative values of $\partial\tau/\partial y$ in the outer layer, and this expectation is confirmed below. Strictly, the mean velocity profile is the result of the entire history of the shear-stress profile, and it is more informative to examine the latter. It does not seem profitable to use the present results to develop sophisticated velocity-profile families with a view to use in 'integral' calculation methods; it is unlikely that a turbulence model based directly on integral parameters would reproduce the effects described below and the use of the Galerkin technique to reduce a 'field' method (partial differential equations) to an 'integral' method (ordinary differential equations) relies for its greater economy on the velocity and shear stress profiles having *simple* shapes, which in the present case they do not.

The shear-stress profiles (figure 11) show a rapid rise in general level through the curved region. The excursions of shear stress near and at the surface are mainly the response to the pressure gradient in the curved region, which necessarily leads to

changes in total pressure at and near the surface: the region in which the flow is in local equilibrium is quite thin, and for $y/\delta > 0{\cdot}1$, say, the shear stress and intensity on a given streamline would remain almost constant through the curved transition region if it were not for the direct effects of curvature and divergence. As it is, the shear stress on the line $y/\delta = 0{\cdot}4$ – roughly a streamline – increases by a factor of nearly 3 through the curved region (i.e. between $s = -159$ and $s = 19$ mm). This behaviour is qualitatively in agreement with that found in I; because the concave-surface flows in I rapidly develop large spanwise inhomogeneities, a quantitative comparison is not possible. Just before the end of the curved transition region, the nominal extra strain rate due to streamline curvature, $-U/R$ where R is the surface radius of curvature, is very nearly equal to the extra strain rate due to lateral divergence, which rises nearly linearly through the bend (figure 2*b*). At the end of the transition section, therefore, the aggregate extra strain rate nominally halves, and thereafter $\partial W/\partial z$ decreases slowly. The curvature of the streamlines is not generally the same as that of the surface and the addition of two components of extra strain rate carries the unjustified implication that their effects are additive, but the plot in figure 2(*b*) is qualitatively helpful. The shear stress also starts to decrease at the end of the transition section but even at the last measurement station, $s = 273$ mm, it is much higher in the outer layer than in a two-dimensional plane flow: it is also much higher than at $x = 310$ in CC20C, the nearest corresponding station in I. Furthermore, while the shear stress in CC20C falls rapidly and monotonically with x after the end of the curved region, the shear stress profile in the present case maintains an almost constant shape between $s = 171$ and $s = 273$, decaying at roughly the rate expected from the slow decrease in $\partial W/\partial z$. Because $\partial W/\partial z$ is decreasing, the shear-stress level at a given station will be slightly higher than if the local value of $\partial W/\partial z$ obtained for all s (the 'time constant' for response of a turbulent boundary layer to perturbation being of order 10δ) but one can be fairly sure that the shape of the shear stress profile at, say, station 24 is principally the result of prolonged divergence, with little memory of the short region of curvature which finished a distance of 15δ upstream.

The collapse of the shear-stress profiles in I was attributed mainly to the large decrease in $\partial U/\partial y$ through the bend, which resulted from the large *increase* in τ (and $\partial\tau/\partial y$) through the bend. The increase in τ in the transition region of the cylinder-flare model is less pronounced than in CC20C (the shear stress at $y/\delta = 0{\cdot}35$ increases by a factor of 2·5 between $s = -159$ and $s = 19$, while in CC20C the factor of increase through the bend is 3·7). An equally significant feature is that the shear-stress peak in the diverging flow moves steadily outwards, while in the two-dimensional concave-surface flow the shear-stress peak, as measured downstream of the bend, remains at about $y/\delta = 0{\cdot}35$ as it decays. In the two-dimensional flow, therefore, the total pressure P increases for $y/\delta < 0{\cdot}35$ and decreases for $y/\delta > 0{\cdot}35$, leading to a large decrease in $\partial U/\partial y$; in the diverging flow $\partial P/\partial x$ at $y/\delta = 0{\cdot}35$ is negative at $s = -32$ and positive for $s = 19$ onwards, and more generally the effects of shear-stress gradients on the U or P profile are smeared out over a larger range of y than in the two-dimensional flow, leading to smaller decreases in $\partial U/\partial y$ and in the shear-stress generation term $\overline{v^2}\partial U/\partial y$. In fact $\overline{v^2}\partial U/\partial y$ decreases very slowly after the end of the bend, in sharp contrast to the precipitous fall found in the case of the 30° concave bend. The direct effect of lateral divergence on $\partial U/\partial y$ is of course significant: first principles, or use of the last term in the transport equation for $\partial U/\partial y$ obtained by differentiating the

x-component momentum equation with respect to y, namely

$$\left(U\frac{\partial}{\partial x}+V\frac{\partial}{\partial y}+W\frac{\partial}{\partial z}\right)\frac{\partial U}{\partial y}=-\frac{1}{\rho}\frac{\partial^2 p}{\partial x\,\partial y}+\frac{1}{\rho}\frac{\partial^2 \tau}{\partial y^2}-\frac{\partial W}{\partial y}\frac{\partial U}{\partial z}+\frac{\partial W}{\partial z}\frac{\partial U}{\partial y}, \tag{2}$$

and substituting $\partial W/\partial z = (U/r)\,dr/dx$, show that the response to a change of cross-sectional radius r is

$$\frac{\Delta\partial U/\partial y}{\partial U/\partial y}=\frac{\Delta r}{r} \tag{3}$$

so that the increase in cross-sectional radius r between the cylindrical body and the flare at $s = 19$ would alone produce an increase in $\partial U/\partial y$ by a factor of about 1·3, depending slightly on the value of y chosen.

The reason for the steady outward progression of the shear-stress peak is, presumably, the continued influence of a destabilizing extra strain rate (i.e. divergence) after the end of the curved transition region; in the two-dimensional flow the extra strain rate falls to zero at the end of the bend. Qualitatively at least, the present flow behaves like the flow in a sharp two-dimensional bend followed by gentler curvature. Whether it is fair to regard this as a nonlinear interaction between curvature and divergence effects is not clear: certainly the effect could be qualitatively reproduced by calculations using linearly additive allowances for the effects of curvature and divergence on turbulence structure, but equally certainly the coupling between the mean flow and the turbulent field via the nonlinear (quasi-linear) shear-stress generation term $\overline{v^2}\partial U/\partial y$ supplies the basic mechanism. Notice that, just as the collapse of shear stress in the concave-surface flows of I was explained without invoking the presence of longitudinal vortices, the absence of the collapse in the present flow need not be attributed to the absence of the vortices. (Certainly one would expect longitudinal vortices to occur in the hypothetical variable-curvature flow mentioned above.)

In the rest of the discussion, it will be taken that the flow at the later stations is dominated by divergence effects, but that the flow in and just downstream of the curved transition region is interesting in itself.

As in I, the intensity profiles (figures 8–10) are best discussed in terms of anisotropy parameters, notably the stress-energy ratio $a_1 \equiv -\overline{uv}/\overline{q^2}$ and the ratios $\overline{v^2}/\overline{u^2}$ and $\overline{uv}/\overline{v^2}$ (figures 15–17: symbols are omitted from these derived figures since the scatter in the data is fairly small as the earlier figures witness). At the first station, $s = -159$, a_1 is close to 0·15 except in the outermost part of the boundary layer. In the bend, it increases uniformly over the outer layer, but as in I the value near the wall is almost unchanged because the ratio of the extra strain rate to $\partial U/\partial y$ is small there (the arguments of § 4.1 of I apply unchanged). Downstream of the bend, values in the inner half of the boundary layer fall rather rapidly with x, to *lower* values than in the initial profile, and values in the outer layer fall more slowly; a_1, like τ, almost reaches a plateau value in the outer layer. The low values in the inner half of the layer are simply explained as the consequences of 'inactive' motion (Townsend 1961; Bradshaw 1967, 1978); the unusually high turbulent activity in the outer part of the flow, where the eddies are large, leads to irrotationally induced motion in the x, z plane near the wall, contributing to $\overline{u^2}$ and $\overline{w^2}$ but not to $\overline{v^2}$ or $\overline{uv}$. A very similar a_1 profile was measured in a strongly retarded boundary layer by Bradshaw (1967): again, the explanation is the high level of turbulence in the outer layer. The value of $\overline{uv}/\overline{v^2}$ (figure 17) is almost

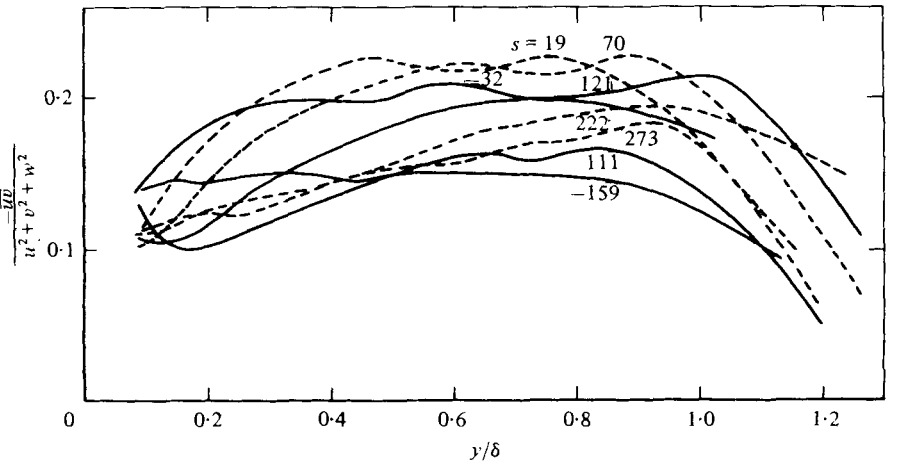

FIGURE 15. Ratio of shear stress to (twice) turbulent energy. The values of s are in mm.

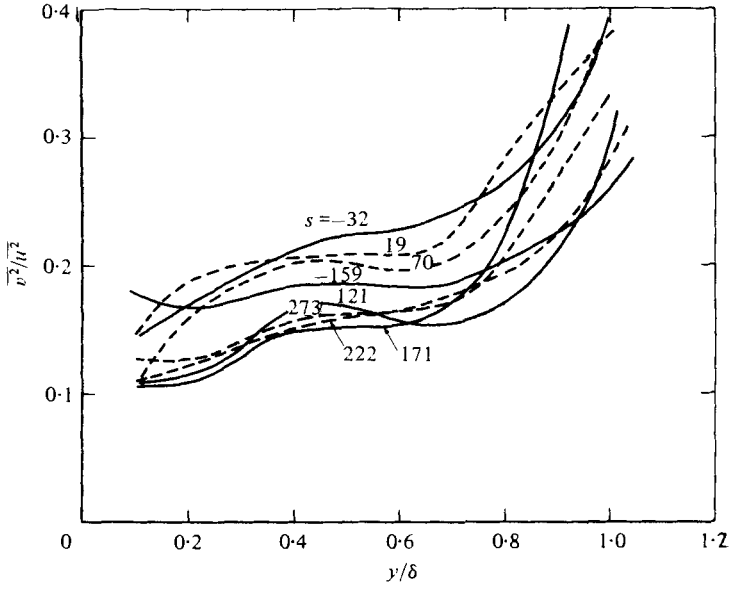

FIGURE 16. Ratio of vertical to longitudinal mean-square intensity. The values of s are in mm.

independent of x in the inner layer, which supports the explanation; in the outer layer $\overline{uv}/\overline{v^2}$ increases, but not so markedly as a_1.

The mixing length and eddy-viscosity profiles (figures 18 and 19) provide rather spectacular demonstrations of the failure of simple turbulence models in complex flows. It is accepted that, being based on local-equilibrium concepts, they fail in rapidly-changing flows, but at the later stations in the present flow the streamwise rates of change are very small: much the same applies to the concave case of I, where streamwise rates of change are even smaller. At $s = 273$, $y/\delta = 0{\cdot}5$, say, the mixing length is about $0{\cdot}16\delta$ or twice the value in a two-dimensional constant-pressure

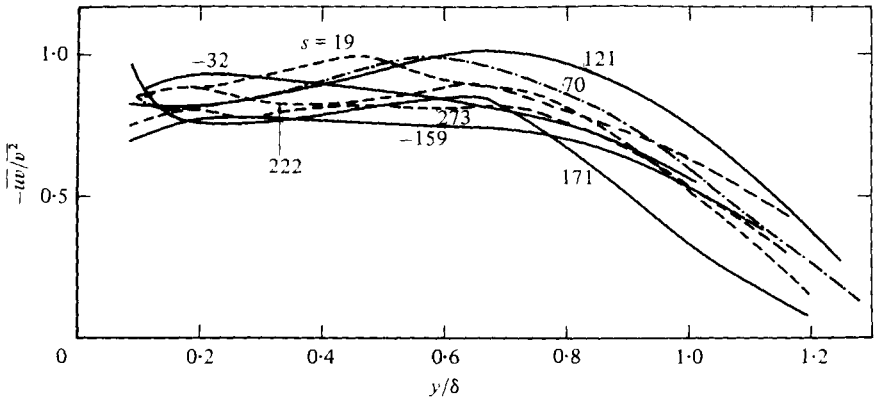

FIGURE 17. Ratio of shear-stress covariance to vertical mean-square intensity. The values of s are in mm.

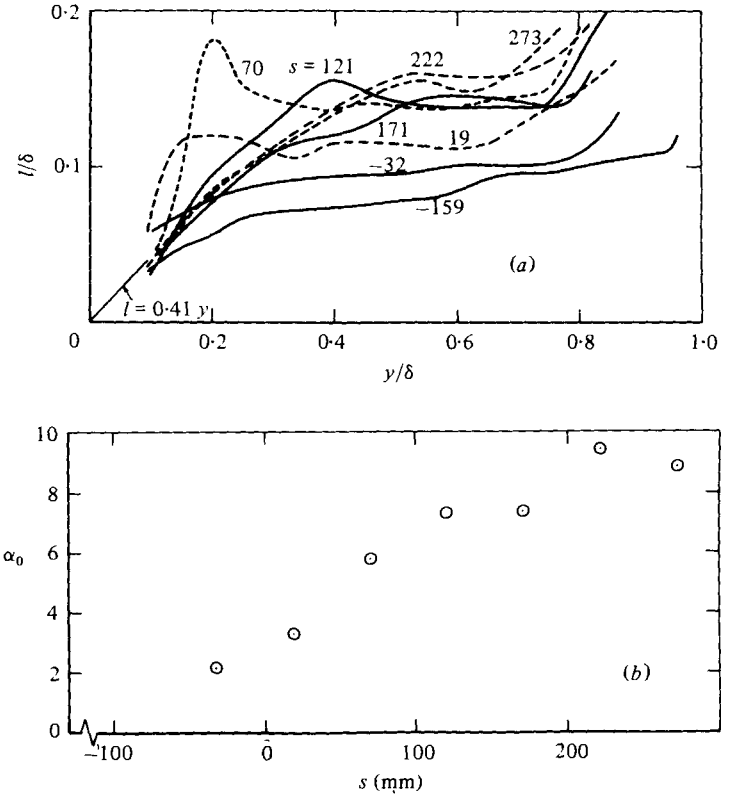

FIGURE 18. 'Mixing length', $l \equiv (-\overline{uv})^{\frac{1}{2}}/(\partial U/\partial y)$. (*a*) Profiles of l/δ, the values of s are in mm. (*b*) Amplification factor α_0 at $y/\delta = 0{\cdot}5$: α_0 is defined by (4) with $e = \partial W/\partial z$.

boundary layer. At this point, $(\partial W/\partial z)/(\partial U/\partial y)$ is about 0·10, which suggests that the empirical constant α_0 in the amplification factor

$$\frac{l}{l_0} = 1 + \alpha_0 e/(\partial U/\partial y) \tag{4}$$

defined in §4.1 of I is nearly 10; other checks at the later stations (figure 18*b*), where the

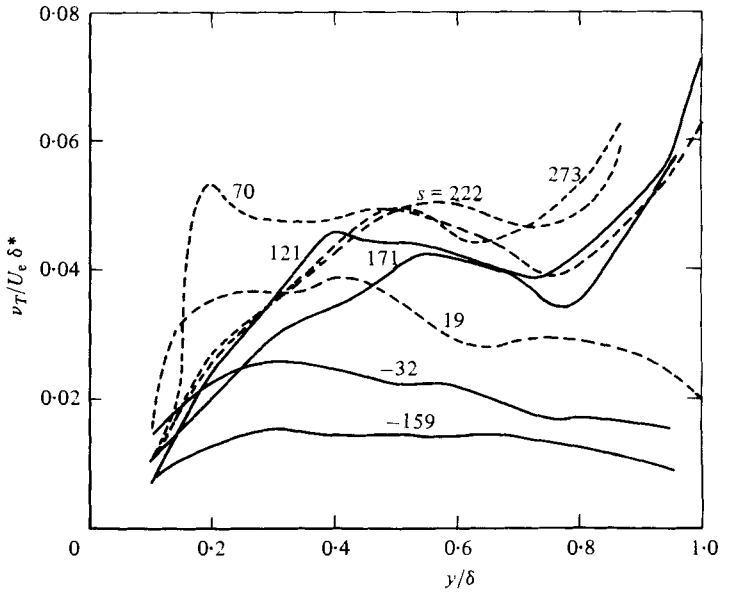

FIGURE 19. 'Eddy viscosity', $\nu_T \equiv -\overline{uv}/(\partial U/\partial y)$.

lag effect mentioned in I is fairly small, also suggest an asymptotic value of about 10 as deduced by Bradshaw (1971) from less detailed data. Near the wall, where extra-strain effects are small, $l \simeq 0{\cdot}41y$ as usual. Note that lag effects have *not* been taken into account in figure 18(*b*); the lag formula should be applied to a true turbulence length scale rather than the mixing length, and analysis of the present results in the context of turbulence modelling will be reported separately. As usual, the variation of eddy viscosity ν_τ is larger than that of mixing length ($\tau \propto \nu_\tau$ but $\tau \propto l^2$).

The triple products (figures 12–14) show an exaggerated version of the rise exhibited by the shear-stress and intensity profiles. Again, a peak forms at $y/\delta \simeq 0{\cdot}3$ and progresses outwards; at the last measurement station the peak in each triple product has reached $y/\delta \simeq 0{\cdot}8$ and the peak value is five or more times the value at the same y/δ in the undisturbed boundary layer. In general the triple-product profiles are much more closely related to the Reynolds-stress profiles than to the Reynolds-stress *gradients*. The extra strain rate evidently augments Reynolds stresses and triple products – and eddy activity in general – in much the same way: in physical terms it augments the outward-going 'bursts' at all positions across the shear layer. An interesting feature, particularly noticeable in $\overline{u^2v}$, is that a secondary peak forms near the wall, entering the measurement region $y/\delta > 0{\cdot}09$ just after the end of the curved transition section and moving outwards until absorbed by the main rise in triple product. Probably the formation of this peak is associated with the relaxation of the large positive shear-stress gradient close to the wall but it could be quantitatively explained by simple gradient-diffusion arguments. As in I, the simplest quantities to discuss are the transport velocities V_q and V_τ (figures 20 and 21). The two main features are the monotonic rise in transport velocity with x in the outer part of the flow, and the fact that, as in I, the transport velocities are positive everywhere, indicating counter-gradient transport in the inner layer. The large but slow increase in transport velocity in response to prolonged extra strain rate is a good demonstration of the

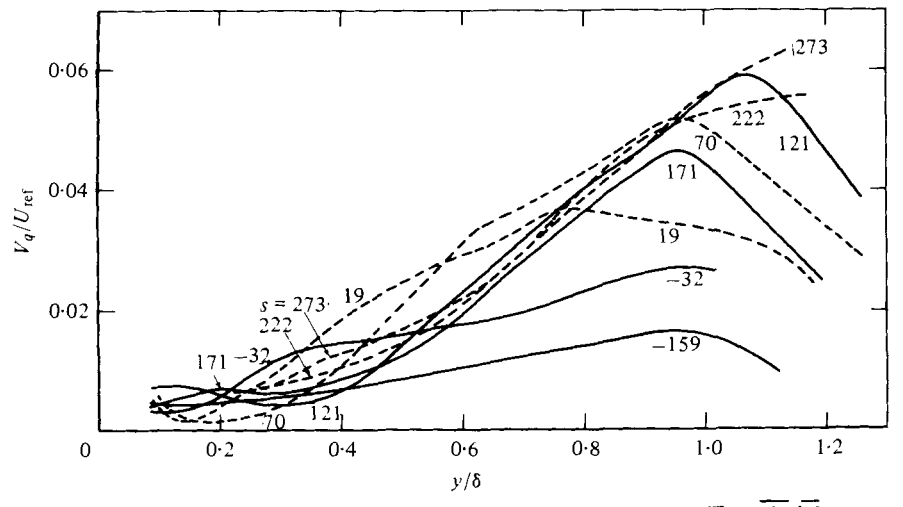

FIGURE 20. Transport velocity of turbulent energy, $V_q \equiv \overline{q^2v}/\overline{q^2}$; $\overline{vw^2}$ assumed equal to $\frac{1}{2}(\overline{u^2v}+\overline{v^3})$.

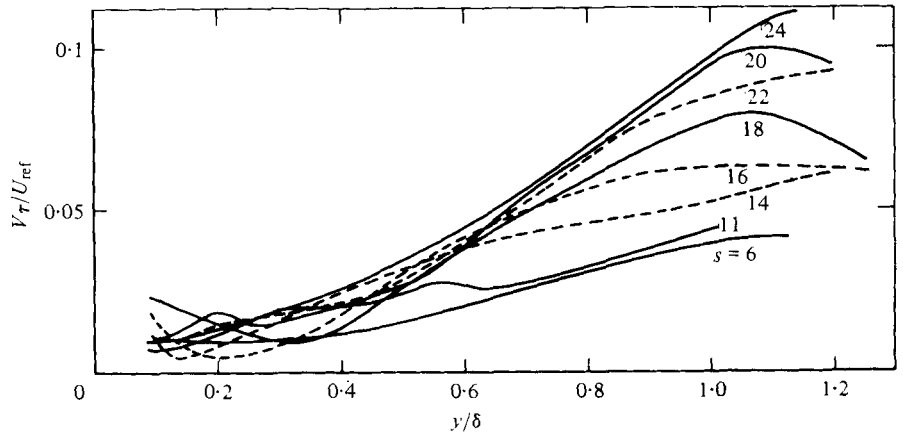

FIGURE 21. Transport velocity of shear stress, $V_\tau \equiv \overline{uv^2}/\overline{uv}$.

long response time of the large eddies in the outer part of a boundary layer, and of the sensitivity of large-eddy structure to extra strain rates. The smoothness of the response suggests that the transport velocities could in principle be correlated by a simple rate equation; the size of the response suggests that such an equation is indeed a necessary part of a calculation method for complex flows like the present one. The simplest view of turbulent transport by the large eddies would suggest that V_q and V_τ should be nearly equal. In fact, V_q/V_τ is well correlated in the present flow, outside the inner region where $V_q/V_\tau \simeq 0$, by $V_q/V_\tau = 3{\cdot}3a_1$ (to be precise, $\overline{uv^2}/\overline{q^2v}$ is close to 0·3, as shown in figure 22) and a_1 (figure 15) varies between 0·15 and 0·2 over the main part of the flow, implying that V_q/V_τ varies between about 0·5 and 0·7. Similar results have been found by Murlis (1975), Castro & Bradshaw (1976) and Andreopoulos (1978).

The entrainment velocity, defined by

$$V_E = \frac{1}{r}\frac{d}{dx}\{rU_e(\delta-\delta^*)\}, \tag{5}$$

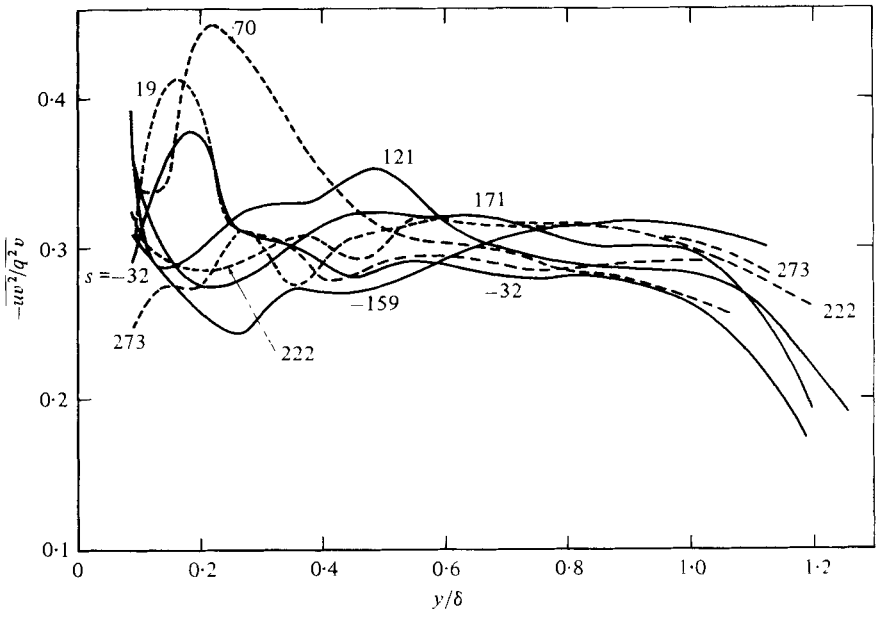

FIGURE 22. Ratio of triple products, $-\overline{uv^2}/\overline{q^2v}$.

is plotted in figure 23. The results in the entry region are ill-defined, and the above relation is not accurate in the curved transition region where thin-shear-layer approximations are not valid. However, the values for about $s > 50$ seem to be reliable and indicate a large increase in entrainment rate: the value for a constant pressure boundary layer at the typical $U_e\,\theta/\nu$ of 5000 is about 0·015, while the peak value in figure 23 is $0{\cdot}046U_e$. If the transport equations reduced to 'mean transport = turbulent transport' near the outer edge of the boundary layer, then the entrainment velocity would equal the y-component turbulent transport velocity: V_q, the transport velocity for turbulent energy, seems to asymptote to a value fairly close to the entrainment velocity, but V_τ (not shown in figure 23) is very much larger, indicating that the sink (pressure-strain 'redistribution') term in the shear-stress transport equation is a large fraction of the turbulent transport term. The decrease in V_E for $s > 100$ seems to be real, but the continued increase in V_q (and V_τ) for $s > 100$ is also well defined; the implication is that the simplifying assumption 'mean transport = turbulent transport' is not to be trusted to great accuracy, at least in strongly perturbed flows like the present one.

Energy balances at a number of stations are presented by Smits, Eaton & Bradshaw (1978). Transport by pressure fluctuations was neglected and dissipation was obtained as the difference of the other terms. Large values of advection occur within and downstream of the bend. The increase in intensity in the inner layer is short lived and stations 14 and 16 show quite large gains by advection (i.e. a decrease of $\overline{q^2}$ in the x direction). Production in mid-layer increases greatly as the shear stress increases; near the wall, the production is nominally $u_\tau^3/(\kappa y)$, and u_τ does not change anything like as rapidly as the shear stress in mid-layer. As well as feeding the advection, the increased production leads to very large increases in diffusion. However the tendency for the triple products to behave like the Reynolds stresses rather than the

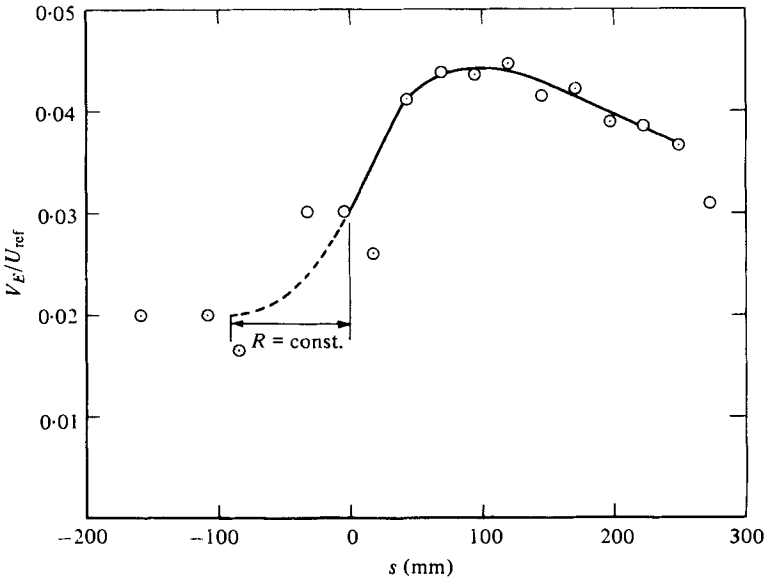

FIGURE 23. Entrainment velocity, $V_E \equiv (1/r)\, d\{U_e r(\delta - \delta^*)\}/ds$.

Reynolds-stress gradients (that is, the tendency for V_q and V_τ to be better behaved than the turbulent diffusivities of $\overline{q^2}$ and $\overline{uv}$) results in quite large *losses* by diffusion from the inner part of the layer as well as from the regions of maximum production.

The values of dissipation ϵ, deduced by difference, have been used to calculate the dissipation length parameter, $L \equiv (-\overline{uv})^{\frac{3}{2}}/\epsilon$, which is plotted in figure 24. Results in the outer layer are very much influenced by the accuracy of the advection, but the general trend of an outward-going peak is clear. If the flow were in local equilibrium, the mixing length l (figure 18) would be equal to L. Values at the last station, $s = 273$, have been omitted; evaluation of the advection at the first or last station is always difficult and honest estimates are manifestly too small (the advection should be about the same as at the previous station) leading to small values of dissipation by difference and hence to excessively large values of L.

Shear-stress balances are also shown by Smits *et al.* (1978). The transport terms are smaller, compared to the source terms, than in the energy balance. The reconciliation of this apparent difference between the energy and shear-stress balances (also found in equilibrium flows) with the relatively simple behaviour of the stress/energy ratio a_1 is that the pressure-strain term consists of two parts. One part, depending on the mean rate of strain, can be thought of as directly opposing the generation term; the second part, independent of the mean velocity field, represents the tendency of the turbulence to return to isotropy. In principle it would be better to group the first (mean-strain dependent) part of the pressure-strain term with the generation term, giving a relatively small net source term which would be roughly balanced by the return-to-isotropy term just as energy production is roughly balanced by dissipation. In practice the mean-strain-dependent part of the pressure-strain term depends on a weighted integral of the mean strain rate over – nominally – the whole flow volume, rather than on local $\partial U/\partial y$, and the weighting function contains complicated

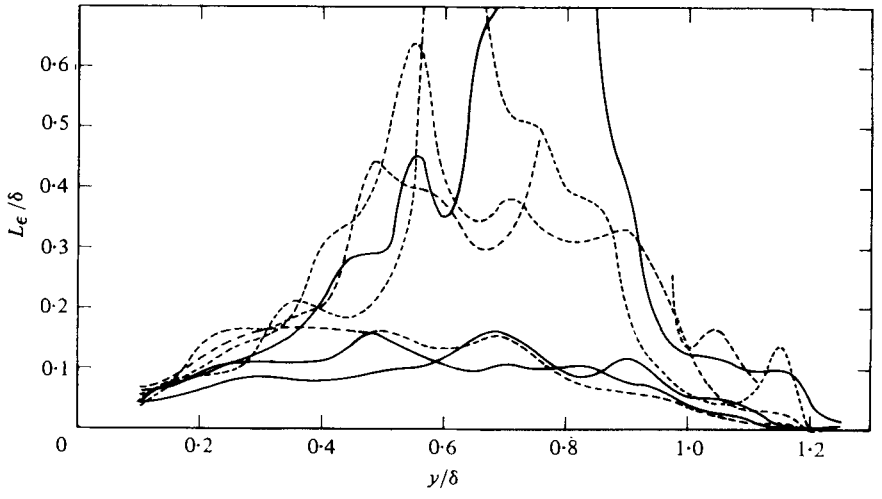

FIGURE 24. Dissipation length scale $L = (-\overline{uv})^{\frac{3}{2}}/\epsilon$.

turbulence quantities which have not yet been measured in any flow. The trends of the terms in the shear-stress balance as listed above are similar to the trends of the corresponding terms in the energy balance. A strong wave of turbulent transport propagates outwards, helping to supply the increase of shear stress in the outer part of the boundary layer in and downstream of the bend (as represented by the mean transport terms). The source of the turbulent transport is the large increase in generation in the region of the peak in $\overline{v^2}$ which leads to a secondary peak in generation in the profiles downstream of the bend. The pressure-strain term increases also but of course it is not possible to divide the increase between the two parts of the term mentioned above.

5. Conclusions

The contrast between the present results and those for the two-dimensional 20° concave bend in I is startling. The contrast seems to depend rather delicately on the way in which the destabilizing effect of extra strain rates varies after the near-impulsive strain imposed by the 20° bend. In the two-dimensional case the extra strain rate disappears at the end of the curved region, leaving a high level of shear stress which has already significantly reduced the mean velocity gradient $\partial U/\partial y$ and continues to do so until shear-stress generation has fallen so much that the turbulence collapses. In the present case the sum of curvature and divergence effects increases through the bend and remains fairly high even after the curvature returns to zero (figure 2*b*). The position of the peak in the shear-stress profile moves steadily outwards, instead of remaining at about the same y/δ, as it does in the two-dimensional bend: as a result, typical values of $\partial U/\partial y$ do not decrease as much as in the two-dimensional case, shear-stress generation remains high and is reinforced by the continuing extra-strain-rate effects, and the turbulence does not collapse. The extra-strain-rate effects in the downstream part of the present flow can be plausibly attributed to prolonged divergence alone. The results show that the empirical constant in the amplification factor for mixing length or similar properties is about 9, the same order as the value for prolonged curvature effects.

This work was supported by Procurement Executive, Ministry of Defence.

REFERENCES

AGRELL, J. & WHITE, R. A. 1974 *FFA, Stockholm, Tech. Note* AU-913.
ANDREOPOULOS, J. 1978 Ph.D. thesis, Imperial College, London.
BANSOD, P. & BRADSHAW, P. 1972 *Aero. Quart.* **23**, 131.
BRADSHAW, P. 1967 *J. Fluid Mech.* **30**, 241.
BRADSHAW, P. 1971 *AGARD Conf. Proc.* 93.
BRADSHAW, P. 1974 *J. Fluid Mech.* **63**, 449.
BRADSHAW, P. 1978 *J. Atmos. Sci.* **35**, 1768.
BRADSHAW, P. & UNSWORTH, K. 1974 *Imperial College, London, Aero. Rep.* 74-02.
CASTRO, I. P. & BRADSHAW, P. 1976 *J. Fluid Mech.* **73**, 265.
COLES, D. E. 1962 *Rand Corp., Santa Monica, Rep.* R-403-PR.
CRABBE, R. S. 1971 *McGill Univ., Mech. Engng Rep.* 71–2.
GREEN, J. E., WEEKS, D. J. & BROOMAN, J. W. F. 1972 *Aero. Res. Counc. R. & M.* 3791.
JOHNSTON, J. P. 1960 *Trans. A.S.M.E.* D **82**, 233.
KEFFER, J. F. 1965 *J. Fluid Mech.* **22**, 135.
KEFFER, J. F. 1967 *J. Fluid Mech.* **28**, 183.
MAHGOUB, H. E. H. & BRADSHAW, P. 1979 *A.I.A.A. J.* (in press).
MURLIS, J. 1975 Ph.D. thesis, Imperial College, London.
PATEL, V. C., NAKAYAMA, A. & DAMIAN, R. 1974 *J. Fluid Mech.* **63**, 345.
REYNOLDS, A. J. 1962 *J. Fluid Mech.* **13**, 333.
RUBESIN, M. W. *et al.* 1977 *A.I.A.A. paper* 77-128.
SMITS, A. J., EATON, J. A. & BRADSHAW, P. 1978 *Imperial College, London, Aero. Rept.* 78-02.
SMITS, A. J., YOUNG, S. T. B. & BRADSHAW, P. 1979 *J. Fluid Mech.* **94**, 209.
TANI, I. 1962 *Geophys. Res.* **67**, 3075.
TOWNSEND, A. A. 1956 *The Structure of Turbulent Shear Flow*, 1st edition. Cambridge University Press.
TOWNSEND, A. A. 1961 *J. Fluid Mech.* **11**, 97.
WINTER, K. G., ROTTA, J. C. & SMITH, K. G. 1968 *Aero. Res. Counc. R. & M.* 3633.